Acta Oceanol. Sin., 2019, Vol. 38, No. 9, P. 128–134
https://doi.org/10.1007/s13131-019-1481-1
http://www.hyxb.org.cn
E-mail: hyxbe@263.net

A multi-channel chemical sensor and its application in detecting hydrothermal vents

Zhen Cai[1], A J Mur Luis[2], Jiwan Han[2], Kui Wang[3, 4], Huawei Qin[5*], Ying Ye[1]

[1] Ocean College, Zhejiang University, Zhoushan 316021, China

[2] Environmental and Rural Sciences, Institute of Biological, Aberystwyth University, Aberystwyth SY23 3DA, UK

[3] Key Laboratory of Marine Ecosystem and Biogeochemistry, State Oceanic Administration, Hangzhou 310012, China

[4] Second Institute of Oceanography, Ministry of Natural Resources, Hangzhou 310012, China

[5] Institute of Mechanical Engineering, Hangzhou Dianzi University, Hangzhou 310018, China

Received 4 August 2018; accepted 23 August 2018

Abstract

There are well-established chemical and turbidity anomalies in the plumes occurring vicinity of hydrothermal vents, which are used to indicate their existence and locations. We here develop a small, accurate multi-channel chemical sensor to detect such anomalies which can be used in deep-sea at depths of more than 4 000 m. The design allowed five all-solid-state electrodes to be mounted on it and each (apart from one reference electrode) could be changed according to chemicals to be measured. Two experiments were conducted using the chemical sensors. The first was a shallow-sea trial which included sample measurements and *in situ* monitoring. pH, Eh, CO_3^{2-} and SO_4^{2-} electrodes were utilized to demonstrate that the chemical sensor was accurate and stable outside the laboratory. In the second experiment, the chemical sensor was integrated with pH, Eh, CO_3^{2-} and H_2S electrodes, and was used in 29 scans of the seabed along the Southwest Indian Ridge (SWIR) to detect hydrothermal vents, from which 27 sets of valid data were obtained. Hydrothermal vents were identified by analyzing the chemical anomalies, the primary judging criteria were decreasing voltages of Eh and H_2S, matched by increasing voltages of pH and CO_3^{2-}. We proposed that simultaneous detection of changes in these parameters will indicate a hydrothermal vent. Amongst the 27 valid sets of data, five potential hydrothermal vents were targeted using the proposed method. We suggest that our sensors could be widely employed by marine scientists.

Key words: chemical sensor, multi-channel, hydrothermal vents detection, chemical anomalies, SWIR

Citation: Cai Zhen, Luis A J Mur, Han Jiwan, Wang Kui, Qin Huawei, Ye Ying. 2019. A multi-channel chemical sensor and its application in detecting hydrothermal vents. Acta Oceanologica Sinica, 38(9): 128–134, doi: 10.1007/s13131-019-1481-1

1 Introduction

Hydrothermal vents are the fissures in the sea floor where underlying heat sources, including magma and hot water, exist (Colín-García et al., 2016), and hydrothermal fluids are generated in the vicinity of them through the interaction of overlying seawater with high-temperature basalt erupting near the seafloor surface. The hydrothermal activity may be a significant component of the chemical mass balance of the oceans due to the substantial amount of particles emitted from hydrothermal vents (Edmond et al., 1982; Mottl and McConachy, 1990). Indeed, particles from hydrothermal plume are known to influence ocean-scale biogeochemical budgets (Breier et al., 2012). Approximately 25% of the earth's heat flux is lost through hydrothermal venting, and the heat loss from venting along mid-ocean ridge can be around 10% (Ramondenc et al., 2006). The environmental temperature near hydrothermal vents is increased due to the heat, which can promote complex chemical reactions (Haymon et al., 1991). Linked to this, hydrothermal vents have been proposed as being the source of critical biochemical reactions that could be associated with the emergence of life on the Earth (Nisbet and Sleep, 2001). Given these aspects, research into hydrothermal venting is a major theme in marine science (German et al., 2016).

Hydrothermal mounds were first observed on the south flank of the Galapagos Rift by DSV Alvin in 1977 (Williams et al., 1979). Submersibles and towed cameras were used to acquire images of hydrothermal vents, and water column sampling was applied to explore the hydrothermal plumes and research their properties. However, the results are limited to the sampling technology, and the water samples may be contaminated in containers or influenced by other factors during the sampling process. The vent field discovery rate using these technologies has been steady at 20 per year since the early 1980s (Baker, 2017). Subsequently, researchers found that hydrothermal plumes could be discovered by real-time measurements of temperature and turbidity (Baker et al., 1985). These were detected by towing corresponding sensors behind a ship to facilitate further explorations by remotely operated vehicles (ROV) or human occupied vehicles (HOV). Using such approaches most high-temperature hydrothermal vent fields with black smokers were easily discovered, but low-temperature or particle-poor vents were likely to be overlooked. In order to overcome the shortcoming, chemical ele-

Foundation item: The Open Foundation of Laboratory of Marine Ecosystem and Biogeochemistry, SOA under contract No. LMEB201701.

*Corresponding author, E-mail: qinhw@hdu.edu.cn

ments, such as sulphide (Rona et al., 1986); CH_4 (Gamo et al., 1993); Mn (Okamura et al., 2001; Provin et al., 2013); Oxidation-Reduction Potential (Eh) (Baker et al., 2010) were used to identify hydrothermal vents based on the research of chemical characteristics of plume. The chemical sensors have been a growing research area over the last few decades. Sensors based on different techniques, such as optical method (McDonagh et al., 2008; Thornton et al., 2015), chemiluminescence method (Okamura et al., 2001) and electrochemical method (Nuzzio et al., 2002), were developed. Now more and more attentions are paid to active higher integration and reduce power consumption. To further ease the process, hydrothermal vents are mapped using instruments mounted on the hull of vessels, such as side-scan sonar (Kumagai et al., 2010), magnetometry equipment (Nakamura et al., 2013), multi-beam devices (Wakita et al., 2010), etc., to scan the seabed's terrain and topography.

This paper describes the development of low power consumption, multi-parameter chemical sensor integrated with five electrodes which can be changed according to the chemicals to be measured in different applications. Two experiments were conducted. The first one was carried in a shallow-sea area to verify the practicability, stability and accuracy of the chemical sensors by *in situ* measurements. In the second experiment, the chemical sensors were applied to the DY-43-III and DY-43-IV cruises, R/V *Xiangyanghong 10* in 2017 to detect hydrothermal vents. Based on the analysis of measured potential data, we identified hydrothermal plumes by extrapolating from the chemical anomalies. The Miniature Autonomous Plume Recorders (MAPRs) equipped with pressure, temperature and optical sensors and conductivity-temperature-depth (CTD) were used to verify the results by measuring physical anomalies. The experiments, therefore, demonstrate chemical sensors and the judging method of the chemicals that can further improve the efficiency of hydrothermal vent exploration.

2 Set-up of the chemical sensor

The chemical sensor is a self-contained instrument which can save measured data to the internal memory chip. It contains a shell, a cap, electrodes and a data acquisition system. The shell is designed to be capable of withstanding high pressures and low temperatures of the deep-sea environment. In our experiments, the shell and cap, which were designed to be used at 4 000 m depths in the sea, were made from a cylindrical titanium alloy. The thickness of the shell is 7 mm, the length of the chemical sensor is about 230 mm, and the diameter is approximately 70 mm. A watertight connector installed on the cap is used to communicate with the computer for setting parameters and reading data, O-ring seals are installed on each thread connection for waterproofing. Figure 1a displays the structure, and Fig. 1b shows the appearance of the chemical sensor.

2.1 *Ion-selective electrode*

The electrochemical measuring method implemented was designed to feature high reproducibility, short response times and high accuracy. Electrodes are the key components which transform chemical information to an electrical signal by the content of selected ions in solution. The concentrations of targeted chemicals are calculated according to the potential difference between the reference electrode and corresponding measuring electrodes. Ion-selective electrodes (ISEs) are preferred in measurements because they can reduce the effects of other ions in solutions. The performance of the ISEs depends partly on the

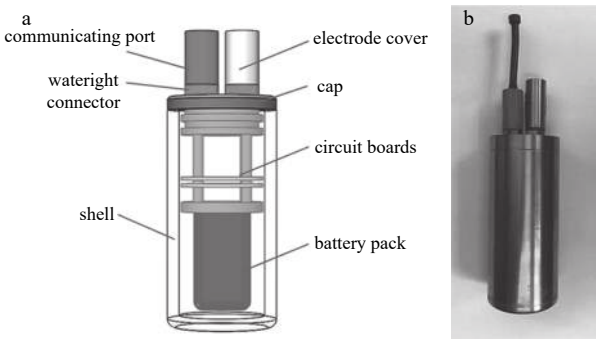

Fig. 1. The developed chemical sensor. a. The structure of the chemical sensor, and b. the appearance of the chemical sensor.

selectivity, which is determined by the nature and composition of the materials. Glass electrodes which contain an internal reference solution are widely used in the electrochemical method (Gonçalves et al., 2011). These electrodes, however, are not suitable for deep-sea applications, because they can easily be damaged in a high-pressure environment. All-solid-statue electrodes, with features of good conductivity, high chemical stability, and anti-corrosion performance, were applied in the experiments. Also, the absence of an internal reference solution makes it possible to integrate with other all-solid-state electrodes easily.

The electrodes were prepared with different approaches according to the ions to be measured. The Eh electrode was a cleaned Platinum electrode (Gillespie, 1920). The Ag/AgCl electrode, as a reference electrode, was fabricated by electrodeposition of AgCl based on the constant current method (Ye et al., 2003). The pH electrode (IrO_x/O_x) was prepared by oxidizing iridium wire based on the mechanism of molten alkali metal carbonate (Pan and Seyfried, 2008). The CO_3^{2-} electrode was fabricated by polydimethylsiloxane (PDMS) gel and Zinc-Aluminium-hydrotalcite (Zn-Al-LDH) ion carrier complex membrane with an Ir/IrO_x electrode as a substrate (Han et al., 2009). The SO_4^{2-} electrode was prepared by aniline hydrochloride served as the active material of sensitive membrane with gold wire (Xing et al., 2017). The H_2S electrode was prepared by the method of carrier electroplating of nano-silver particles (Ding et al., 2015). The detection limits of CO_3^{2-}, SO_4^{2-} and H_2S electrodes were 10^{-4}, 10^{-4} and 10^{-5} mol/L respectively. The lifespans of Ag/AgCl, CO_3^{2-}, SO_4^{2-} and H_2S electrodes were 60, 5, 10, 6 d, respectively. The relationships between the output potentials generated by electrodes to the solution concentrations were calibrated by the electrochemical workstation CHI660E (Shanghai Chenhua Instrument Co., Ltd) in the laboratory with a room temperature at a constant 25°C. The KQ218 ultrasonic cleaning machine (Kunshan Ultrasonic Instruments Co., Ltd) was used to clean the electrodes. The structure of electrodes mounted on the watertight connector is shown in Fig. 2.

2.2 *Data acquisition system*

The data acquisition system, consisting of analog and digital circuit parts with corresponding computer software, was designed to acquire and save data. The default storage cell in the digital circuit part is one page comprising 40 rows of data. During the data saving procedure, the Microcontroller Unit (MCU) packs data into one page and saves it to the flash memory each time the data row number reaches 40. The redundant data whose total line number is less than 40 will be abandoned when the last page

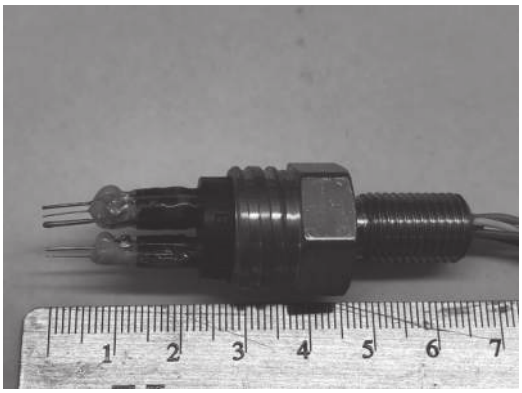

Fig. 2. The photograph of five electrodes mounted on the watertight connector, one of them is the reference electrode, and the other four electrodes are changeable according to chemicals to be measured.

is saved. The printed circuit boards (PCB) are shown in Fig. 3.

Due to limitations of space within the interior of the shell, there is little volume available for the battery. To lengthen battery life, low power consumption electronic components and a highly efficient Li-ion battery pack, consisting of four batteries, were used. The nominal voltage of one battery is 3.6 V, and its nominal capacity is 4 000 mAh, so the nominal capacity of the battery pack is 16 Ah. To extend this, a sleeping mode was developed based on the features of the MCU to decrease power consumption when the system is not in operation. The main electronic components and their power consumption are shown in Table 1.

There are slight delays from the moment that electrodes are electrified to the outputting of stable signals, as a result of the different response time of each electrode. To obtain accurate potentials, the electrifying method for the electrodes was improved, in which the electrifying time of electrodes is changed based on the sampling frequency set by the users. Electrodes are electrified during measurements when the sample rate is greater than 0.1 Hz (the sample interval is less than 10 s), and when the sample rate is less than 0.1 Hz, the electrodes are electrified one second ahead of sampling. The battery's performance at different sampling intervals is shown in Table 2.

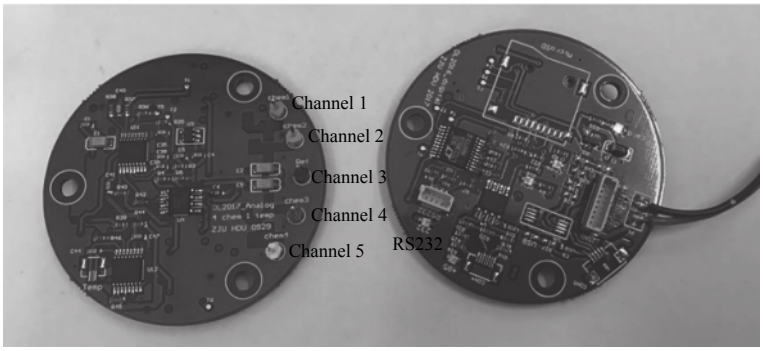

Fig. 3. The PCBs of the data acquisition system, which includes an analog circuit part (left) and a digital circuit part (right). In the analog circuit part, there are five channels used to connect electrodes. In the digital circuit part, there is an RS232 communication port used for communicating with the computer.

Table 1. The main electronic components and their power consumption

Type	Model	Main power consumption
MCU	MSP430F169	40 μA in low power mode
Real-time lock	PCF8563	<200 μA
Flash memory	AT45DB321B	I/O:4 mA, static state: 3 μA
RS232	LTC1385	200 mA

Table 2. The battery performance at different sample intervals

Sample interval/s	Power consumption per day/mV	Measuring time/d
5	72	11.1
30	59	13.5
60	34	23.5
120	18	44.4

3 Shallow-sea trial and results

3.1 *The shallow-sea trial*

In order to test the performance of the chemical sensor in seawater containing a large number of interfering ions, a shallow-sea preliminary trial was conducted in the area near Goutoushan Island, Taizhou (29°03′23.4″N, 121°39′53.1″E) on 26 September 2016. The complex chemical environment exists in this area, as it is an aquaculture zone where seawater and freshwater from the Jiaojiang River mix. The pH, Eh, CO_3^{2-} and SO_4^{2-} electrodes were applied in the trail. Before the measurement commenced, the output potential of the electrodes was calibrated by using corresponding buffer solutions with different concentrations at the environmental temperature of 25°C. For example, pH buffer solutions of 4.25, 7.0 and 10.02 were used to calibrate the pH electrode, and the potentials of 286.8 mV, 166.79 mV and 46.15 mV were obtained, respectively. Then the calibration curve (Fig. 4a) was calculated using least square method according to the pH values and the potentials (E). Na_2SO_4 solutions (10^{-4} mol/L to 10^{-1} mol/L) were used to calibrate the SO_4^{2-} electrode (Fig. 4b), and Na_2CO_3 solutions (10^{-4} mol/L to 10^{-2} mol/L) were used to calibrate the CO_3^{2-} electrode (Fig. 4c). To examine the reproducibility of the fabricated electrodes, each electrode was calibrated four times, the standard deviations of correlation coefficients (R^2) of pH, SO_4^{2-} and CO_3^{2-} electrodes are 0.001 5, 0.003 1 and 0.001 5, respectively.

The chemical sensors were tied to a buoy with a ~1 m string, and the electrodes of the chemical sensor were orientated up-

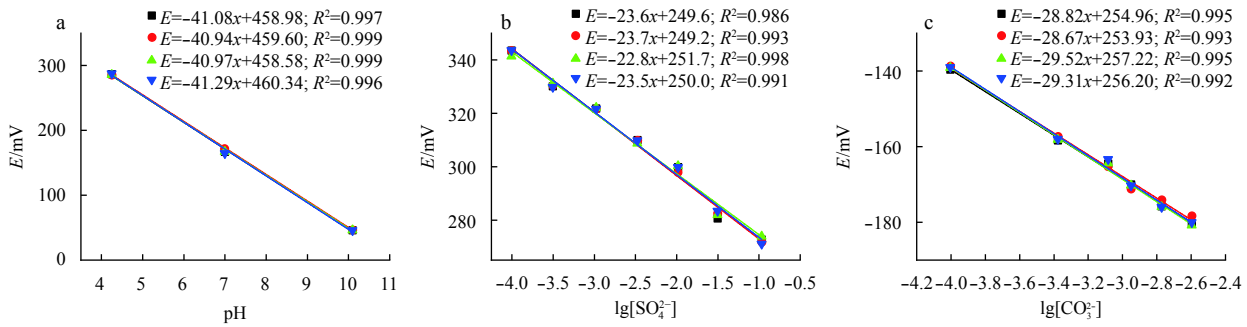

Fig. 4. The calibration curves of the electrodes used in the shallow-sea trial. a. The pH electrode in pH buffer solutions of 4.25, 7.0 and 10.02; b. the SO_4^{2-} electrode in solutions whose Na_2SO_4 concentration range of 10^{-4}–10^{-1} mol/L; and c. the CO_3^{2-} electrode in solutions whose Na_2CO_3 concentration range of 10^{-4}–10^{-2} mol/L.

wards to reduce the influence of disturbed seabed silt. Seawater samples near the chemical sensor were collected three times for subsequent assays, and the sampling time was recorded. The voltage data were obtained via the RS232 communication port after 10 hours of *in situ* measurement and were converted to concentrations of corresponding ions using the calibration equations shown in Fig. 4.

3.2 *Results of the shallow-sea trial*

The results determined by different methods are shown in Table 3. The pH values of the samples determined by pH meter were 8.08, 8.09 and 8.08 respectively. This corresponded with the pH value measured at the same time by the pH electrode of the chemical sensor of 8.11, and the maximum difference was 0.03. The SO_4^{2-} ion concentration of the water sample was determined using the gravimetric method, and the values were 1.93 g/L, 1.93 g/L and 1.91 g/L, respectively, while the value measured by the chemical sensor was 1.89 g/L. The concentrations of the CO_3^{2-} ion, as determined by the titration, were 15.51 mg/L, 14.76 mg/L and 15.13 mg/L, respectively, and the result measured by the chemical sensor was 14.82 mg/L. The preliminary trial demonstrated that the chemical sensors could be used in complex chemical environments, and the similarity between the measured results implied that the electrodes were accurate for practical applications.

Table 3. Results determined by gravimetric method, titration method and chemical sensors

	Value			Chemical sensor	
	Sample 1	Sample 2	Sample 3	Value	Standard deviation
pH	8.08	8.09	8.08	8.11	0.015 81
$[SO_4^{2-}]$/g·L^{-1}	1.93	1.93	1.91	1.89	0.011 55
$[CO_3^{2-}]$/g·L^{-1}	15.51	14.76	15.13	14.82	0.020 82

4 Hydrothermal vents detection experiment and results

4.1 *The hydrothermal vents detection experiment*

There are various substances in the surrounding areas of hydrothermal plumes, some of which can be used to indicate their existence. The detection of chemicals which are the most common and have apparent change near hydrothermal vent fields is the preferred approach, and our choice of electrodes was influenced by these considerations. The potential of Eh has been used as an indicator since the mid-1990s, because it is sensitive to reduced chemicals (such as H_2S and Fe^{2+}) existing in hydrothermal plumes. A sharp decline of the Eh value occurs when the Eh electrode contacts the short-lived reduced chemicals. The reduced chemicals rapidly oxidize close to the seafloor after they are emitted from hydrothermal vents. Thus, greater Eh anomalies indicate the younger parts of plumes, which are closer to the source (Walker et al., 2007). The Eh sensors have often been used in hydrothermal vent explorations associated with turbidity sensors (Baker et al., 2010; Ray et al., 2012). Our experiments sought to detect hydrothermal vents using chemical sensors, so other chemicals were also measured to improve reliability. One of the reduced chemicals, H_2S, was measured using Ag/Ag_2S electrode, and the increasing concentration of S^{2-} ion decreases the potential of Ag/Ag_2S electrode. Additionally, the concentration of CO_3^{2-} ion around the hydrothermal plume areas is lower than in other areas. Therefore, pH, Eh, H_2S and CO_3^{2-} electrodes were integrated into the chemical sensor for hydrothermal vents detection.

Tests were conducted before the deep-sea experiment to ensure the pressure-bearing performance of the shell. The maximum pressure was set to 60 MPa, equivalent to the pressure in seawater at a depth of 6 000 m. In the first test, two assembled chemical sensors were both kept in the pressure vessel at 60 MPa for ten minutes; then gradually reduced to barometric pressure. This procedure was repeated nine times to verify their pressure bearing performance. Subsequently, these two chemical sensors were kept in the 60 MPa vessel for 60 min to verify the long-term pressure bearing performance.

For the DY-43-III and DY-43-IV cruises, the chemical sensors were mounted on the towed body attached to the R/V *Xiangyanghong 10*. To measure turbidity at different depths of hydrothermal plumes, turbidity transducers (MAPRs and CTDs) were fixed on the cable with different distances to the towed body. The turbidity transducer (device number RBR67) was mounted on the towed body. The distances from the towed body to the other turbidity sensors mounted on the cable (device numbers were RBR76, MAPR94 and MAPR92) were 200 m, 150 m and 70 m, respectively. Figure 5a is a diagram of the installation of devices and measurements. Figure 5b shows the photograph of the chemical sensor on the towed body with turbidity sensors.

During the whole cruise, chemical sensor measurements were conducted 29 times (11 times in the DY-43-III and 18 times in the DY-43-IV) in the sea area of SWIR. The SWIR is a mid-ocean ridge located along the Rodrigues triple junction (RTJ) in the Indian Ocean and Bouvet triple junction (BTJ) in the Atlantic Ocean, and it separates the African and Antarctic plates. The

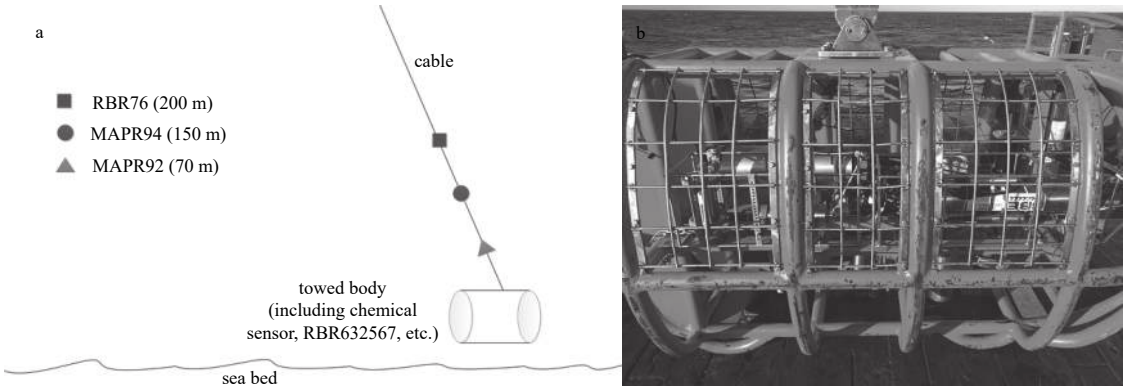

Fig. 5. The schematic diagram of the measurement. a. Device installations on the towed body, and b. the photograph of the towed body which was equipped with the chemical sensor and turbidity sensors.

SWIR is characterized by the extremely slow spreading rate (1.4–1.6 cm/a) (Tao et al., 2014), which is an essential factor in the morphology of mid-ocean ridges. The geophysical data show that the thickness of the earth's crust, topography, mantle composition and magmatic activity of the SWIR vary from BTJ to RTJ. Many hydrothermal vents have been discovered in the SWIR since the 1990s. For example, six hydrothermal anomalies were discovered during the Fuji cruise in 1997 (Fujimoto, 1999). Highly tectonized areas, which are deemed to be favourable for hydrothermal activity, were targeted during the Indoyo cruise in 1998 (Münch et al., 2001). Hydrothermal deposits recovered by dredging from an oblique segment of the SWIR between 10° and 16°E were discovered in the Knorr cruise 162 (Banerjee et al., 2001).

The sample rates of chemical sensors and turbidity transducers were set to 0.2 Hz, the speed of the towed body was 1.5 kn, and 27 sets of valid data were obtained, two sets of data were abandoned due to the illegal operations during measurement.

4.2 *Results and discussion*

As the amount of the chemicals and particles of hydrothermal plumes differs from non-plume water, it was expected that there would be sudden changes of the potential data at the boundary of hydrothermal plume fields, and there would be variations when the sensors were moving in these areas. Such sudden changes and variations of the potential can be used to confirm the existence of hydrothermal vents. We developed our sensor to be an accurate and reliable detector of such changes so that it could have wide applicability in marine research. The derived sensor was tested in the deep-sea experiment, and the obtained data were not converted to concentrations but analyzed as row potential data. The adjacent averaging method of 15 points was used to reduce random error and noise.

The measurements of 43III-SWIR-L001-SHX01 were conducted on 25 February 2017. The towed body and the cable equipped with measuring instruments (one chemical sensor and four turbidity sensors) were put into the sea at 03:00 and the towed body reached the seabed at 04:11, where the depth of this site was 2 043 m. Retrieval began at 15:00, so valid data obtained from 04:11 to 15:00 and the potentials are shown in Fig. 6.

The potential of Eh decreased from 04:11, and it was not stable until 07:00. However, the potentials of pH and H_2S were relatively stable throughout this period, and the changes were not apparent in comparison with Eh value. The decrease of Eh value

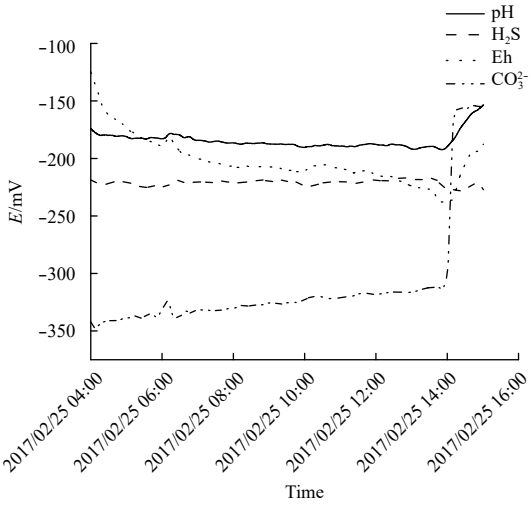

Fig. 6. The potentials of pH, Eh, CO_3^{2-} and H_2S measured by the chemical sensor in the measurement of 43III-SWIR-L001-SHX01.

and the increase of H_2S concentration usually appear simultaneously near hydrothermal vents. Hence, this decrease of Eh value is likely to reflect the measurement of reduced substances not originating from hydrothermal plumes. The potential of Eh began to descend at 11:46, and rapidly reduced to 9 mV at 13:40, indicating that the chemical reducibility of this site was increasing. As the potential of H_2S dropped to 10 mV, the concentration of H_2S was increasing. During the same period, the gradual increase in potential linked to pH indicated elevated acidity. The sharply rising potential from the CO_3^{2-} electrode shows that the concentration of the CO_3^{2-} ion was changed quickly. However, this change exceeds the range of CO_3^{2-} ion in hydrothermal vent fluids, which is mainly caused by the electrode drift in the plume. Higher resolution data from 13:00 to 14:45 are shown in Fig. 7a. In order to reduce the effects of drift and hysteresis, the time derivative, dE/dt, was calculated to identify the chemical anomalies. The time derivatives of corresponding potentials are shown in Fig. 7b. Taken together this chemical anomalies demonstrate that the towed body was in the area of hydrothermal plume field during the period. We spent about one-hour collecting sulfide samples in this area by TV-Grab, and the towed body was retrieved when the collections were finished. Therefore, the potentials of electrodes were still affected by the chemical components

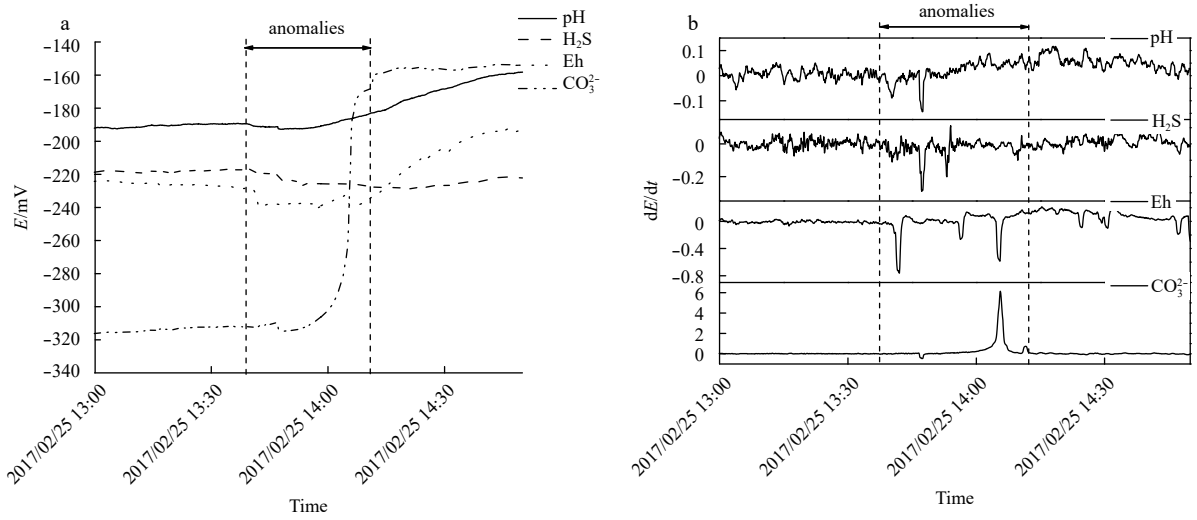

Fig. 7. The detail results from 11:30 to 15:00. a. the measured potential data, and b. the differences of corresponding potential data.

of the plume.

The turbidity data recorded by turbidity sensors were analyzed to verify the detection result by the chemical sensor (Fig. 8). During the period when chemical anomalies were detected, turbidity increases of 0.012 NTU were detected by RBR67 (on the towed body), and of 0.007 NTU by both MAPR92 (70 m from the towed body) and MAPR94 (150 m from the towed body). However, there is no apparent anomaly detected by RBR76 (200 m from the towed body). The degree of detected turbidity varied with the distance between the turbidity sensors and towed body. Thus, the closer to the towed body, the more turbidity anomalies were detected, as the hydrothermal vents are formed near seafloors. As the cable in measurements was not vertical to sea level, the turbidity was first detected by the furthest sensor. Moreover, the position of the hydrothermal vent detected by the chemical anomalies agrees with that of Tao et al. (2014).

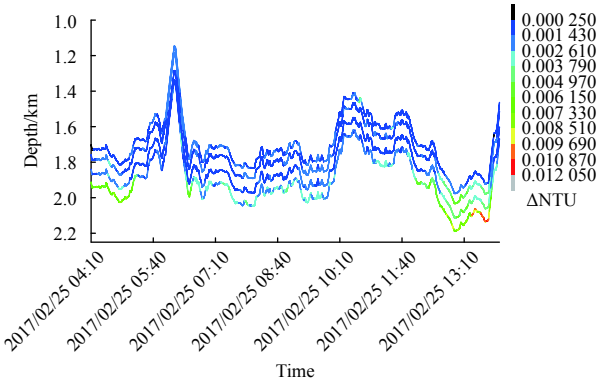

Fig. 8. Turbidity data at different depths from 04:11 to 14:00 measured by the turbidity sensors.

According to the analyses above, the existence of hydrothermal vents can be confirmed by the chemical anomalies measured by the developed chemical sensor. The decreasing potentials of Eh and H_2S, which we suggest is the primary judging criterion as well as the increasing potentials of pH and CO_3^{2-}. We propose that simultaneous satisfaction of all these four indices will reduce most incorrect judgments of hydrothermal vent positions. Another 26 sets of data measured by the chemical sensor were analyzed according to the proposed judging method, and four potential hydrothermal vents are confirmed. The details are shown in Table 4.

Table 4. The results of the DY-43-III and DY-43-IV cruises

Cruise	Measurement	Valid data set	Potential hydrothermal vents
DY-43-III	11	10	2
DY-43-IV	18	17	3

5 Conclusions

Hydrothermal vents are the keys to understanding many chemical, biological and physical processes in the deep sea. In this paper, a low power consumption chemical sensor was developed to detect hydrothermal vents by measuring chemical anomalies of plumes. The chemical sensor contains a shell, cap, electrode and data acquisition system. It assembles five electrodes including one Ag/AgCl reference electrode whose output potential is used as a reference signal, and four other electrodes can be changed according to the chemicals to be measured in various applications. The battery performance and pressure-bearing performance were tested for prolonged measurements under deep sea conditions.

Before detecting hydrothermal vents, a shallow-sea preliminary trial was performed in the sea area near Goutoushan Island which contains determinations of water samples and 10 h of *in situ* monitoring. The pH, Eh, CO_3^{2-} and SO_4^{2-} electrodes were used, and the results show that the chemical sensors are accurate, suitable and practical in applications. Then, the chemical sensors were applied to the DY-43-III and DY-43-IV cruises, R/V *Xiangyanghong 10* for hydrothermal vent detection. The pH, Eh, CO_3^{2-} and H_2S electrodes were used during the experiment, and 27 sets of valid data were obtained from the 29 measurements. According to the analyses of measured chemical data, the chemical anomalies (the sharp decline of Eh value, the decreasing potential of H_2S, and the increasing potentials of pH and CO_3^{2-}) were used to confirm the existence of hydrothermal vents. All the 27 sets of data were analyzed, and five potential hydrothermal vents were confirmed. The chemical sensor also can there be

used in other applications.

References

Baker E T. 2017. Exploring the ocean for hydrothermal venting: New techniques, new discoveries, new insights. Ore Geology Reviews, 86: 55–69, doi: 10.1016/j.oregeorev.2017.02.006

Baker E T, Lavelle J W, Massoth G J. 1985. Hydrothermal particle plumes over the southern Juan de Fuca Ridge. Nature, 316(6026): 342–344, doi: 10.1038/316342a0

Baker E T, Martinez F, Resing J A, et al. 2010. Hydrothermal cooling along the Eastern Lau Spreading Center: No evidence for discharge beyond the neovolcanic zone. Geochemistry, Geophysics, Geosystems, 11(8): Q08004

Banerjee R, Dick J B H, Wolfgang B. 2001. Discovery of peridotitehosted hydrothermal deposits along the ultraslow-spreading Southwest Indian Ridge. In: Geological Society of America annual meeting. Boston, 800

Breier J A, Toner B M, Fakra S C, et al. 2012. Sulfur, sulfides, oxides and organic matter aggregated in submarine hydrothermal plumes at 9 50′ N East Pacific Rise. Geochimica et Cosmochimica Acta, 88: 216–236, doi: 10.1016/j.gca.2012.04.003

Colín-García M, Heredia A, Cordero G, et al. 2016. Hydrothermal vents and prebiotic chemistry: a review. Boletín de la Sociedad Geológica Mexicana, 68(3): 599–620, doi: 10.18268/BSGM2016v68n3a13

Ding Qian, Pan Yiwen, Huang Yuanfeng, et al. 2015. The optimization of Ag/Ag_2S electrode using carrier electroplating of nano silver particles and its preliminary application to offshore Kueishan Tao, Taiwan. Continental Shelf Research, 111: 262–267, doi: 10.1016/j.csr.2015.08.018

Edmond J M, Von Damm K L, McDuff R E, et al. 1982. Chemistry of hot springs on the East Pacific Rise and their effluent dispersal. Nature, 297(5863): 187–191, doi: 10.1038/297187a0

Fujimoto H. 1999. First submersible investigations of mid-ocean ridges in the Indian Ocean. Inter Ridge News, 8: 22–24

Gamo T, Sakai H, Ishibashi J, et al. 1993. Hydrothermal plumes in the eastern Manus Basin, Bismarck Sea: CH_4, Mn, Al and pH anomalies. Deep Sea Research Part I: Oceanographic Research Papers, 40(11–12): 2335–2349, doi: 10.1016/0967-0637(93)90108-F

German C R, Petersen S, Hannington M D. 2016. Hydrothermal exploration of mid-ocean ridges: where might the largest sulfide deposits be forming? Chemical Geology, 420: 114–126, doi: 10.1016/j.chemgeo.2015.11.006

Gillespie L J. 1920. Reduction potentials of bacterial culture and of water-logged soils. Soil Science, 9(4): 199–216, doi: 10.1097/00010694-192004000-00001

Gonçalves M A, Gonzaga F B, Fraga I C S, et al. 2011. Evaluation study of different glass electrodes by an interlaboratory comparison for determining the pH of fuel ethanol. Sensors and Actuators B: Chemical, 158(1): 327–332, doi: 10.1016/j.snb.2011.06.029

Han Chenhua, Pan Yiwen, Ye Ying. 2009. CO_2 microelectrode based on Zn-AI-LDH-ion carrier and its characterization. Journal of Tropical Oceanography (in Chinese), 28(4): 35–41

Haymon R M, Fornari D J, Edwards M H, et al. 1991. Hydrothermal vent distribution along the East Pacific Rise crest (909′–54′ N) and its relationship to magmatic and tectonic processes on fast-spreading mid-ocean ridges. Earth and Planetary Science Letters, 104(2–4): 513–534, doi: 10.1016/0012-821X(91)90226-8

Kumagai H, Tsukioka S, Yamamoto H, et al. 2010. Hydrothermal plumes imaged by high-resolution side-scan sonar on a cruising AUV, Urashima. Geochemistry, Geophysics, Geosystems, 11(12): Q12013

Münch U, Lalou C, Halbach P, et al. 2001. Relict hydrothermal events along the super-slow Southwest Indian spreading ridge near 63° 56′ E-mineralogy, chemistry and chronology of sulfide samples. Chemical Geology, 177(3–4): 341–349, doi: 10.1016/S0009-2541(00)00418-6

McDonagh C, Burke C S, MacCraith B D. 2008. Optical chemical sensors. Chemical Reviews, 108(2): 400–422, doi: 10.1021/cr068102g

Mottl M J, McConachy T F. 1990. Chemical processes in buoyant hydrothermal plumes on the East Pacific Rise near 21 N. Geochimica et Cosmochimica Acta, 54(7): 1911–1927, doi: 10.1016/0016-7037(90)90261-I

Nakamura K, Toki T, Mochizuki N, et al. 2013. Discovery of a new hydrothermal vent based on an underwater, high-resolution geophysical survey. Deep Sea Research Part I: Oceanographic Research Papers, 74: 1–10, doi: 10.1016/j.dsr.2012.12.003

Nisbet E G, Sleep N H. 2001. The habitat and nature of early life. Nature, 409(6823): 1083–1091, doi: 10.1038/35059210

Nuzzio D B, Taillefert M, Cary S C, et al. 2002. In situ voltammetry at deep-sea hydrothermal vents. In: Taillefert M, Rozan T F, eds. Environmental Electrochemistry. Washington, D C: American Chemical Society, 811: 40–53

Okamura K, Kimoto H, Saeki K, et al. 2001. Development of a deep-sea in situ Mn analyzer and its application for hydrothermal plume observation. Marine Chemistry, 76(1–2): 17–26, doi: 10.1016/S0304-4203(01)00043-3

Pan Yiwen, Seyfried W E Jr. 2008. Experimental and theoretical constraints on pH measurements with an iridium oxide electrode in aqueous fluids from 25 to 175 C and 25 MPa. Journal of Solution Chemistry, 37(8): 1051–1062, doi: 10.1007/s10953-008-9293-z

Provin C, Fukuba T, Okamura K, et al. 2013. An integrated microfluidic system for manganese anomaly detection based on chemiluminescence: Description and practical use to discover hydrothermal plumes near the Okinawa Trough. IEEE Journal of Oceanic Engineering, 38(1): 178–185, doi: 10.1109/JOE.2012.2208849

Ramondenc P, Germanovich L N, Von Damm K L, et al. 2006. The first measurements of hydrothermal heat output at 950′ N, East Pacific Rise. Earth and Planetary Science Letters, 245(3-4): 487–497, doi: 10.1016/j.epsl.2006.03.023

Ray D, Kamesh R K A, Baker E T, et al. 2012. Hydrothermal plumes over the Carlsberg Ridge, Indian Ocean. Geochemistry, Geophysics, Geosystems, 13(1): Q01009

Rona P A, Klinkhammer G, Nelsen T A, et al. 1986. Black smokers, massive sulphides and vent biota at the Mid-Atlantic Ridge. Nature, 321(6065): 33–37, doi: 10.1038/321033a0

Tao Chunhui, Li Huaiming, Jin Xiaobing, et al. 2014. Seafloor hydrothermal activity and polymetallic sulfide exploration on the southwest Indian ridge. Chinese Science Bulletin, 59(19): 2266–2276, doi: 10.1007/s11434-014-0182-0

Thornton B, Takahashi T, Sato T, et al. 2015. Development of a deep-sea laser-induced breakdown spectrometer for in situ multi-element chemical analysis. Deep Sea Research Part I: Oceanographic Research Papers, 95: 20–36, doi: 10.1016/j.dsr.2014.10.006

Wakita N, Hirokawa K, Ichikawa T, et al. 2010. Development of Autonomous Underwater Vehicle (AUV) for exploring deep sea marine mineral resources. Mitsubishi Heavy Industries Technical Review, 47(3): 73–80

Walker S L, Baker E T, Resing J A, et al. 2007. A new tool for detecting hydrothermal plumes: An ORP Sensor for the PMEL MAPR. In: American Geophysical Union, Fall Meeting. Washington DC: American Geophysical Union

Williams D L, Green K, Van Andel T H, et al. 1979. The hydrothermal mounds of the Galapagos Rift: Observations with DSRV Alvin and detailed heat flow studies. Journal of Geophysical Research: Solid Earth, 84(B13): 7467–7484, doi: 10.1029/JB084iB13p07467

Xing Liang, Kang Yating, Zhou Yifan, et al. 2017. Determination of sulfate in seawater by a novel all-solid-state sulfate sensor with H_2SO_4 doped polyaniline as sensitive membrane. International Journal of Electrochemical Science, 12(2): 1506–1520

Ye Ying, Wu Daidai, Huang Xia, et al. 2003. Preparation and performance characterization of novel solid pH sensing electrodes. Journal of Transcluction Technology (in Chinese), 16(4): 487–490